Nanoscale

Cite this: *Nanoscale*, 2012, **4**, 3359

www.rsc.org/nanoscale

PAPER

Plasmonic near-field in the vicinity of a single gold nanoparticle investigated with fluorescence correlation spectroscopy

Guowei Lu,*[a] Jie Liu,[a] Tianyue Zhang,[a] Wenqiang Li,[a] Lei Hou,[a] Chunxiong Luo,[a] Franck Lei,[b] Michel Manfait[b] and Qihuang Gong*[a]

Received 31st December 2011, Accepted 26th March 2012
DOI: 10.1039/c2nr12137a

We proposed the estimation of the plasmonic near-field volume in the vicinity of a single gold nanoparticle, and observed experimentally the near-field variation due to a change in the polarization of the illuminating light. Under total-internal-reflection illumination, the plasmonic near-field volume is varied by tuning the polarization of the excitation light. The variation in the optical near-field around a single gold nanoparticle was simulated theoretically with a finite-difference time domain method, and was characterized experimentally employing a fluorescence correlation spectroscopy technique. The experimental results are in agreement quantitatively with the theoretical analysis. These results are highly relevant to important efforts to clarify the interaction between the emitter and the plasmonic antenna, and should be helpful in developing a plasmonic-enhanced total-internal-reflection fluorescence imaging microscope.

Introduction

Plasmonic optical antennas by metallic nanostructures can efficiently concentrate light into a deep-subwavelength volume.[1] This unique feature is currently of tremendous interest to researchers investigating a broad range of emerging applications, from chemical and biomolecular sensing to energy harvesting to subwavelength optical imaging.[2–4] To realize these applications, it is critical to quantify the optical field distribution when light is concentrated in the vicinity of the antenna. Gold spherical nanoparticles (AuNPs), with diameters of several tens of nanometers, are simple and widely used optical antennas.[5–7] Although both analytical and numerical theoretical methods can provide a physically intuitive image of the optical field distribution in the vicinity of a AuNP, few studies have measured experimentally such a plasmonic near-field around an optical nano-antenna on the scale of several tens of nanometers. High-resolution techniques such as scanning near-field optical microscopy employing an aperture or apertureless probe,[8,9] electron-energy-loss spectroscopy,[10] two-photon luminescence microscopy,[11] and cathodoluminescence microscopy[12,13] can spatially map the relative variations in the plasmon modes within antennas or the optical field strength near antennas. However, experimental methods to extract the characteristics of the local optical field near AuNPs on the scale of tens of nanometers are lacking. A full understanding of the plasmonic near-field of AuNPs would help us design or optimize many applications related to plasmonics in terms of the interaction between molecules and the plasmonic nanostructure.

Furthermore, the localized surface plasmon resonance response of the nano-antennas and the related surface-enhanced spectroscopy (*e.g.* surface-enhanced Raman scattering and plasmonic-enhanced fluorescence) near the antennas are usually polarization dependent. For instance, a single AuNP attached to a tapered fiber apex as an optical antenna has been precisely controlled under scanning probe microscopy to investigate the plasmonic effect of the AuNP on the behavior of single-molecule fluorescence.[6,7] Experimental and theoretical results are consistent with each other, and the plasmonic-enhanced near-field extends tens of nanometers around the AuNP surface. Simply, the single molecule can be considered as a tiny probe that senses the plasmonic near-field in the vicinity of an individual AuNP. However, the local optical field near single AuNPs under different conditions of illumination polarization has not been reported in the literature. It is probable that the fluorescent molecules in previous experiments were fixed in a solid matrix and only molecules aligned along the direction of the excitation light could be detected efficiently; otherwise, the signal is weak when the polarization of the illumination changes.

In this study, an isolated AuNP immobilized on a glass coverslip is illuminated by a total-internal-reflection evanescent optical field. The field distribution near a single AuNP is simulated employing a finite-difference time domain (FDTD).[14] Under illumination by linear polarized light, the field distribution around the AuNP presents two lobes where the plasmonic

[a]*Department of Physics, State Key Laboratory for Mesoscopic Physics, Peking University, 100871 Beijing, China. E-mail: guowei.lu@pku.edu.cn; qhgong@pku.edu.cn*
[b]*Unité MéDIAN, UMR CNRS 6237, UFR Pharmacie, Université de Reims Champagne-Ardenne, 51 rue Cognacq-Jay, 51096 Reims cedex, France*

enhanced near optical field is aligned along the direction of excitation polarization as indicated in Fig. 1. For P-polarized illumination, one of the two lobes penetrates the glass substrate. Therefore, the plasmonic near-field excitation volume illuminated by P-polarized light should be smaller than that illuminated by S-polarized light when the fluorescent solution specimen exists only on the glass substrate. Additionally, the plasmonic near-field excitation intensity differs for different cases of linear polarized illumination. To the best of our knowledge, there has been no reported investigation of such tiny variation in the plasmonic near-field near a single AuNP.

Here, an aqueous solution of fluorescent dye provides a uniform probe distribution around the AuNPs. Since the fluorescent molecules can diffuse and rotate freely in the aqueous solution, the disadvantages of molecule photobleaching and orientation effects are overcome. A quasi single-molecule technique using an aqueous solution (*i.e.* fluorescence correlation spectroscopy (FCS))[15] is proposed to investigate the plasmonic near-field in the vicinity of a single AuNP under various conditions of polarized illumination light. FCS has been successfully applied to calibrate detection volumes over the optical diffraction limit; *e.g.* the nanoscale detection volume generated by stimulated emission depletion,[16] the confined effective volume generated by metallic nano-apertures,[17–19] and near-field effects of nanoparticles.[20–22] Our results will show that the variation in the plasmonic near-field volume around a single AuNP under different conditions of polarized light can be estimated quantitatively by FCS. Additionally, the fluorescence enhancement effect is stronger for S-polarized illumination. These results are highly relevant to important efforts to understand the optical properties of a plasmonic antenna, and have potential applications for total-internal-reflection fluorescence imaging in biological analysis.

Experimental and methods

Fig. 2 shows our objective-type total-internal-reflection fluorescence correlation spectroscopy (TIR-FCS) setup based on the NTEGRA Spectra system (NT-MDT, Russia). The beam of a HeNe laser (CW laser, λ: 633 nm) is enlarged using a telescope

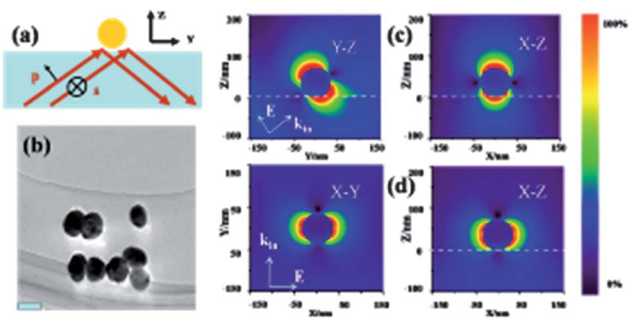

Fig. 1 (a) Schematic diagram of total-internal-reflection optical illumination in the presence of a AuNP. (b) TEM image of the synthesized AuNPs used in this experiment; the scale bar is 50 nm. (c) and (d) Electric field intensity distributions simulated by employing a 3D FDTD around a AuNP under the illumination of P-polarized and S-polarized incident light, respectively. Simulation of a AuNP with a diameter of 70 nm; the cell size of the FDTD calculation is 2 nm × 2 nm × 2 nm.

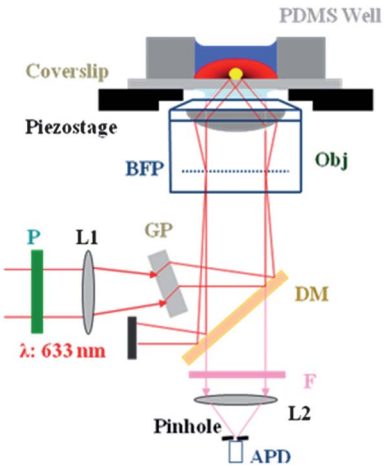

Fig. 2 Schematic diagram of the experimental setup: P, wave plate; GP, glass plate; DM, dichroic mirror; F, fluorescence filter; L1, L2, lenses.

and then focused at the back focal plane (BFP) of an oil-immersion objective lens (NA = 1.49, 60×, Olympus, Japan) by lens L1 with focal length 400 mm. By tilting the glass plate (GP) as indicated in Fig. 2, the location of the focal spot can be adjusted within the BFP to ensure that the collimated beam emerging from the objective impinges on the glass–water interface at an inclination critical angle sufficient to introduce the total internal reflection. A $\lambda/2$ wave plate (P) is used to adjust the polarization of the incident illumination light. In this experiment, S, P, and circularly polarized incident light are used separately to vary the plasmonic near-field excitation volume around a single AuNP as indicated in Fig. 1. The fluorescence signal is collected by the same objective lens and then focused by tube lens L2 (focal length 180 mm) onto the end of a fiber with a core diameter of 50 μm after passing through a dichroic mirror and a bandpass emission filter (LPD01-633RU, FF01-661/20-25, Semrock) used to block the diffuse reflected laser light. The core of the fiber acts as a pinhole, ensuring the confinement of the observation volume. A 50/50 fiber splitter is used to send the signal to two avalanche photodiodes (SPCM-AQRH-16-FC, PerkinElmer) for cross-correlation to suppress afterpulsing (correlator.com, US).

The gold colloid nanoparticles of diameter 60 ± 10 nm are synthesized through citrate reduction in this work.[23] The surfactant 3-aminopropyl-trimethoxysilane (APTMS) is used to immobilize the AuNPs on the glass surface.[24] In brief, the glass coverslips are carefully cleaned ultrasonically before undergoing oxygen plasma treatment, and they are then immersed in 10% (v/v) APTMS solution for 15 minutes. After silanization of the glass surface, a droplet containing AuNPs is deposited onto the APTMS functionalized coverslip surface, and left for ~1 minute to sparsely cover the AuNPs. Finally, the coverslips are washed thoroughly with ethanol and water to remove the unbound AuNPs. To hold the aqueous solution of fluorophores, a polydimethylsiloxane liquid well is connected to the coverslip after the immobilization of AuNPs upon the surface. The sample is treated with oxygen plasma to prevent unspecific dye molecules from binding before the TIR-FCS measurements.

The FCS method is based on the fluctuation of the fluorescence intensity F_t. The autocorrelation function (ACF) is defined as

$$G(\tau) = \langle F_t \cdot F_{t+\tau} \rangle / \langle F \rangle^2, \quad (1)$$

where $\langle\rangle$ denotes a time-averaged value and τ is the lag time. For a single freely diffusing fluorophore in solution, F_t can be expressed as

$$F_t = \int Q_r \cdot I_r \cdot C_{r,t} \mathrm{d}V, \quad (2)$$

where Q_r is defined as the product of the absorption cross section and the fluorescence quantum yield; I_r is the intensity distribution profile determined by both the excitation and detection optical paths; and $C_{r,t}$ is the local concentration. For TIR-FCS, the model based on the theoretical description given by Thompson is widely used with a transversal diffusion function:[25,26]

$$G(\tau) = 1 + \frac{1}{2N}(1 - \langle B \rangle / \langle F \rangle)^2 \left[1 + p_{\mathrm{T}} \exp\left(-\frac{\tau}{\tau_{\mathrm{T}}}\right)\right] \left(1 + \frac{\tau}{\tau_{xy}}\right)^{-1} \times \left[\left(1 - \frac{\tau}{2\tau_z}\right) \exp\left(\frac{\tau}{4\tau_z}\right) erfc\left(\sqrt{\frac{\tau}{4\tau_z}}\right) + \sqrt{\frac{\tau}{\pi\tau_z}}\right]. \quad (3)$$

N is the number of dye molecules in the effective detected volume with $V_{\mathrm{eff}} = \pi\omega_{xy}^2 d$, where ω_{xy} is the lateral extent of the Gaussian intensity distribution confined by a pinhole and d denotes the axial distance, where the intensity decreases exponentially to 1/e. $\langle B \rangle$ is the background noise that can be measured from the pure water without any fluorophore dye, and $\langle F \rangle$ is the total fluorescence signal. p_{T} is the amplitude of the dark-state population caused by *trans–cis* isomerization and singlet–triplet transition processes within τ_{T}, the corresponding blinking time. $\tau_z = \frac{d^2}{4D}$, $\tau_{xy} = \frac{\omega_{xy}^2}{4D}$ are the diffusion times for the directions vertical and parallel to the surface, respectively, and D is the diffusion coefficient.

In the presence of a AuNP, the intensity of molecule fluorescence in the vicinity of the AuNP increases at a certain distance from the nanoparticle surface, where the plasmonic enhanced fluorescence dominates the quenching effect.[6] Thereby, Q_r and I_r should differ when the AuNP is within the illumination focus, compared to the case where there is no AuNP. As an approximation, it is convenient to introduce a simple constant enhancement factor ρ_r while deriving the autocorrelation function. The detected fluorescence intensity can thus be written as

$$F_t = \int Q_c (I_{1,r} + \rho_r \cdot I_{2,r}) C_{r,t} \mathrm{d}V. \quad (4)$$

Here, the profile of the excitation light is separated into two parts: $I_{1,r}$ represents the profile induced directly by the total-internal-reflection evanescent field, while $I_{2,r}$ is the plasmonic near-field in the vicinity of the AuNP. We approximate this plasmonic near-field volume as a Gaussian distribution around the nanoparticle surface. Q_c is assumed to remain constant as in a free open solution. The autocorrelation function is then obtained as

$$G(\tau) = 1 + \frac{1}{2N}\left[1 + p_{\mathrm{T}} \exp\left(-\frac{\tau}{\tau_{\mathrm{T}}}\right)\right] \frac{(1 - \langle B \rangle / \langle F \rangle)^2}{(2N_1 + \rho_{\mathrm{r}} N_2)^2} \left\{ \frac{2N_1}{1 + \tau/s_1^2\tau_1} \times \left[\left(1 - \frac{\tau}{2\tau_1}\right) \exp\left(\frac{\tau}{4\tau_1}\right) erfc\left(\sqrt{\frac{\tau}{4\tau_1}}\right) + \sqrt{\frac{\tau}{\pi\tau_1}}\right] + \frac{N_2}{(1 + \tau/\tau_2)\sqrt{1 + \tau/s_2^2\tau_2}} \right\}. \quad (5)$$

Here, N_2 is the number of fluorescent molecules within the plasmonic near-field region around the AuNP and $V_2 = \pi^{3/2}\omega_{2-p}^2\omega_{2-v}$. The subscripts p and v represent the directions parallel and vertical to the surface of the particle, respectively. N_1 is the number of fluorescent molecules in the evanescent volume, illuminated at the glass–water interface by far-field total internal reflection and confined by the system pinhole, where

$$V_1 = \pi\omega_{1-xy}^2 d, \tau_1 = \frac{d^2}{4D}, \tau_2 = \frac{\omega_{2-p}^2}{4D}, s_1 = \omega_{1-xy}/d, s_2 = \omega_{2-v}/\omega_{2-p}.$$

Although several approximations have been made already while deriving the autocorrelation function in the presence of the AuNP, the formula is still so complex that it is difficult to extract an accurate and reliable value of the parameters by fitting the whole of the measured ACF curves and the plasmonic near-field information in the vicinity of the AuNP. Fortunately, the problem can be circumvented by careful analysis of the $G(0)$ value. We can deduce the relative effective detection volume according to

$$G(0) = 1 + (1 + p_{\mathrm{T}})(1 - \langle B \rangle / \langle F \rangle)^2 \frac{2N_1 + \rho_{\mathrm{r}}^2 N_2}{(2N_1 + \rho_{\mathrm{r}} N_2)^2}. \quad (6)$$

The effective detection volume and the number of molecules within it can be obtained from the $G(0)$ value, even though the whole ACF curve is not fitted very well. $G(0)$ is independent of the shape of the excitation field and the type of molecular diffusion, and its validity holds for a stationary system and a dilute solution, where the spatial correlation length of concentration fluctuations is much smaller than the dimensions of the detection volume.[15,16] Here, we define

$$\beta = \frac{1}{\alpha} \cdot \frac{G_{\mathrm{Au}}(0) - 1}{G_0(0) - 1} = \frac{4 + 2\rho_{\mathrm{r}}^2 N_2/N_1}{(2 + \rho_{\mathrm{r}} N_2/N_1)^2}, \quad (7)$$

where the subscript Au denotes the presence of a AuNP and the subscript 0 denotes the absence of a AuNP.

$$\alpha = \frac{1 + p_{\mathrm{T,Au}}}{1 + p_{\mathrm{T,0}}} \cdot \left(\frac{1 - \langle B_{\mathrm{Au}} \rangle / \langle F_{\mathrm{Au}} \rangle}{1 - \langle B_0 \rangle / \langle F_0 \rangle}\right)^2, \quad (8)$$

where $N_1 = C_{r,t} V_1$, determined by the molecule concentration, and the total-internal-reflection evanescent detection volume is assumed to approximately remain equal to N in the absence of the AuNP. Fig. 3 shows β as a function of N_2/N_1 (*i.e.* the ratio of the molecule numbers within the AuNP's plasmonic near-field to that in the total-internal-reflection evanescent detection volume) for different values of ρ_r. The inset of Fig. 3 shows that β monotonously increases as the ratio of N_2/N_1 increases, when the ratio is less than 0.01 (there is a turning point at ~0.05), and then β reduces as the ratio increases after the turning point.

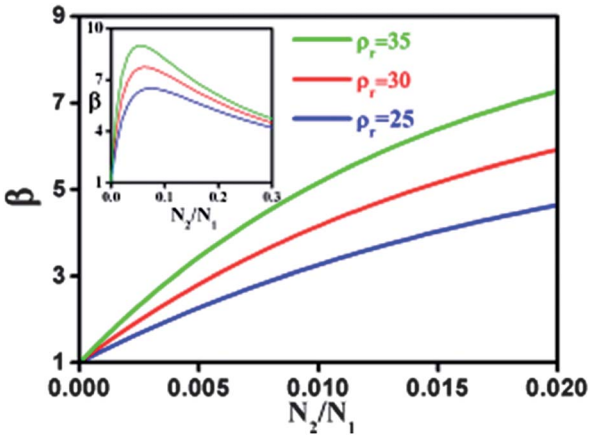

Fig. 3 The factor β as a function of the ratio of N_2/N_1; red curve, $\rho_r = 35$; blue curve, $\rho_r = 30$; green curve, $\rho_r = 25$.

For TIR-FCS in the presence of a single AuNP, the plasmonic near-field volume in the vicinity of the nanoparticle with a diameter of ~60 nm should be less than a factor of 0.05 of the TIR evanescent detection volume confined by the pinhole and the objective lens. Then, N_2/N_1 should be less than 0.05 in this situation, given that the concentration of dye molecules has a uniform distribution, irrespective of the presence of a AuNP. For simplicity, the enhancement factor ρ_r is approximated as a constant, owing to the highly symmetric structure of the gold nanoparticle, although it is dependent on the distance and orientation.[5,27] Thus, by comparing β measured under different conditions of polarized illumination, the change in and relative scale of the plasmonic near-field volume can be easily estimated.

Results and discussion

In this work, TIR-FCS measurements were made for the 50 nM Cy5 aqueous solution. The power intensity of the incident laser was kept at 10 mW as measured before the lens L1. For comparison, the TIR-FCS ACF curves for differently polarized excitation light were firstly measured for the bare coverslip surface (*i.e.* without AuNPs). Fig. 4 shows the typical ACF curves recorded in the absence of the AuNP under different conditions of polarized light. First, the fluorescence intensity varies for differently polarized illumination as shown in the inset of Fig. 4. This is mainly due to the difference in the excitation intensity; *i.e.* the reflection efficiency of the dichroic mirror and transmission efficiency at the glass–water interface differ for variously polarized light.[28] Nevertheless, the autocorrelation curves are almost the same, which implies that the intensity distribution profiles for different polarizations are similar. This has been demonstrated in many previous studies, and it is also found for different excitation laser powers (data not shown here). The fitting of the ACF curves with eqn (1) shows that $\tau_z = 10.9 \pm 2.5$ μs and $\tau_{xy} = 110 \pm 30$ μs. Assuming that ω_{xy} is about 400 nm, the evanescence depth d is obtained as ~125 nm; these results are reasonable and acceptable.

With the help of an optical scanning stage based on the NETGRA Spectra system, TIR-FCS measurements can be made easily with high spatial accuracy in the presence or absence of the

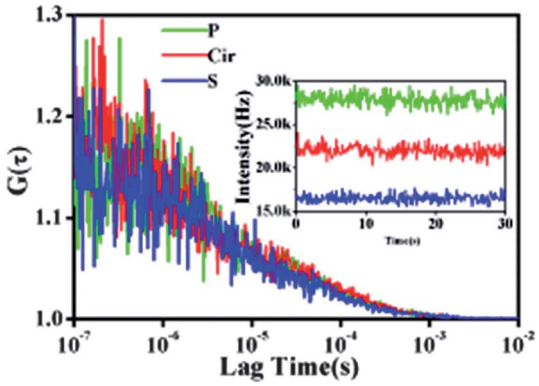

Fig. 4 Typical ACF curves for 50 nM Cy5 solution illuminated by differently polarized light in the absence of the AuNP. The blue plot is the results for S-polarization, the red plot the results for circular polarization, and the green plot the results for P-polarization. The inset shows time traces of the fluorescence intensity measured separately for differently polarized light.

AuNP. The results in the presence of the AuNP differ obviously from those in the absence of the AuNP as shown in Fig. 5. Firstly, the fluorescence intensity in the presence of the AuNP is higher than that without a nanoparticle. Additionally, there are obvious strong bursts in the time traces of fluorescence intensity, which are probably due to the diffusion of dye molecules into the plasmonic near-field around the AuNP where the molecule fluorescence is plasmonic-enhanced significantly. Secondly, there is a distinct increase in the $G(0)$ value in the presence of the AuNP, and β also increases as expected. This is in accordance with the results of previous studies, where researchers have observed the near-field effect of an individual AuNP, employing the confocal-FCS method.[20,22] The increase in the $G(0)$ value indicates that either fewer molecules (*i.e.* fewer than $N_1 + N_2$) are detected, or an additional source of fluorescence fluctuation affects the FCS autocorrelation curves. The physical reduction in the detection volume in the presence of an AuNP is much less than the effective far-field detection volume. The effect of the physical reduction on the total detection volume is less than 1%

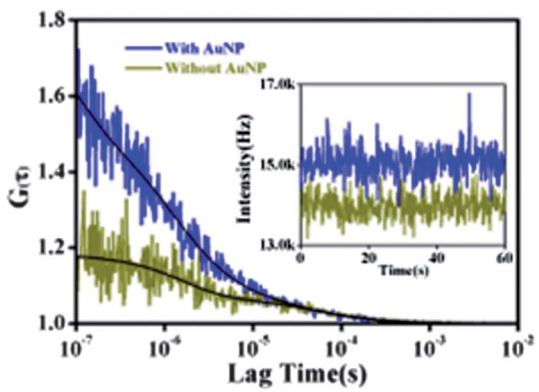

Fig. 5 Typical TIR-FCS ACF curves measured in the presence of the AuNP (blue) and in the absence of the AuNP (brown), under S-polarized illumination. The black curves are the fitting lines obtained with eqn (3) and (5) separately. The inset shows time traces of the fluorescence intensity. The concentration of the Cy5 aqueous solution is 50 nM.

and should only result in a tiny increase in the β value. The supplementary source of the fluctuations can be attributed to the random diffusion of the dye molecules around the AuNP. It has already been found that the quenching and enhancement of single-molecule fluorescence near a AuNP depends on distance.[6,7] Therefore, the emission from the dye molecule can be enhanced or quenched when the molecules diffuse near the AuNP, which results in an obvious fluctuation of the fluorescence signal. This fluorescence fluctuation occurs around the plasmonic near-field of the AuNP with a characteristic dimension of tens of nanometers, and the diffusion time scale is thus around a microsecond. This time scale overlaps the time scale of the dark-state fluctuation caused by the *trans–cis* isomerization and singlet–triplet transitions. Thus, it is difficult to extract a reliable value simply by fitting the ACF curves, although the curves can be fitted with eqn (2).

Nevertheless, as we see from Fig. 6, the $G(0)$ values measured under different conditions of polarized incident light are obviously different, and the value for S-polarized incident light is highest. Because of the asymmetric glass–water interface, the effective detected near-field volume around the gold nanoparticle varies under different conditions of polarized excitation light. Additionally, as predicted by FDTD simulation, the excitation plasmonic near-field volume illuminated by S-polarized incident light is about twice that illuminated by P-polarized incident light. As discussed above, this deviation in the near-field volume will affect the ACF curves. The $G(0)$ and β values then increase because the near-field volume is less than a factor of 0.05 of the regular TIR evanescence excitation volume. This is a clear demonstration by experiment, rather than through theoretical simulation, that the plasmonic near-field excitation volume differs under various conditions of polarized illumination. Given that the enhancement factor is the same for S-and P-polarized illumination and the near-field volumes differ by a factor of ~2 as predicted by FDTD simulation, the relative plasmonic near-field volume is a factor of ~0.003 of the TIR evanescent volume, which is consistent with the result in the literature,[20] taking into account the fact that the TIR evanescent volume is about an order of magnitude smaller than the regular Gaussian confocal focus volume. Additionally, the fluorescence enhancement is obtained roughly as a factor of around 30–35 according to Fig. 3. This fluorescence enhancement factor agrees with the value reported in the literature.[6]

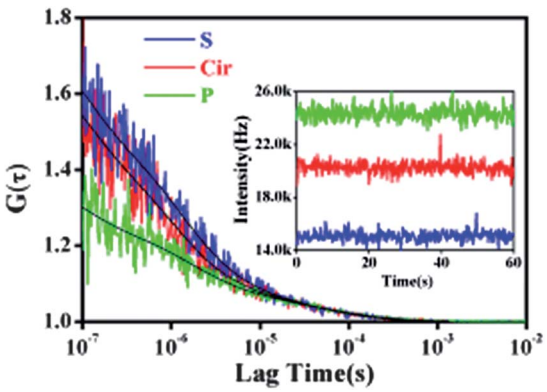

Fig. 6 Typical TIR-FCS ACF curves measured in the presence of the AuNP with differently polarized light. The blue plot is the results for S-polarization, the red plot is the results for circular polarization, and the green plot is the results for P-polarization. The black curves are the fitting lines obtained using eqn (5). The inset shows the corresponding time traces of fluorescence intensity.

Furthermore, the difference in the effective near-field volume also should be reflected in the variation in fluorescence intensity. As shown in Table 1, the increase in the normalized fluorescence intensity due to S-polarized incident light is obviously higher than (more than twice) that due to P-polarized incident light (for comparison, TIR-FCS measurements are also made on the bare glass surface under different conditions of polarized light). The normalized enhancement of fluorescence intensity is still higher for S-polarized incident light, even though the effect on the number of molecules due to the variation in the near-field volume is taken into account. This result infers that the enhancement factor ρ_r is indeed different for different conditions of polarized incident light. The exponential decay of the optical field near the water–glass interface is likely the main reason for the difference in enhancement efficiency. As shown in Fig. 1, the separation of the plasmonic near-field volume from the water–glass interface is larger under P-polarized illumination than under S-polarized illumination. Moreover, the fluorescence enhancement should relate to the emitter's orientation and the emission direction, which are factors modulated by the plasmonic nanostructure.[5,27] More efforts are needed to clarify this point, but they are beyond the scope of this study.

To this end, the results show that S- and circularly polarized light provide a greater enhancement effect, while P-polarized light leads to a smaller excitation volume. We believe that the present results can be used to improve the performance of total-internal-reflection fluorescence microscopy (TIRFM), which is a useful technique still under development, and used widely to investigate events near an interface in the field of biological imaging. For instance, an imaging technique that combines surface plasmon cross emission within a TIRFM configuration, adding a thin metallic film on the glass substrate, is called surface plasmon enhanced-TIRFM, and it has been used recently in the imaging of muscle fibrils.[29,30] Thus, the effect of illumination polarization has to be considered when designing plasmonic-enhanced fluorescence microscopy.

Conclusions

We measured experimentally the variation in the plasmonic near-field excitation volume in the vicinity of a single AuNP under different conditions of polarized illumination. Under total-internal-reflection illumination, the plasmonic near-field effective

Table 1 Measured fluorescence intensity and the corresponding factor β under different conditions of polarized illumination. The background signals have been deducted already

Polarization	Without AuNP (F_1)/kHz	With AuNP (F_2)/kHz	$(F_2 - F_1)/F_1$	β
S	13.5	14.3	0.056	3.5
Cir	18.5	19.5	0.054	3.1
P	23.7	24.1	0.019	1.8

volume can be changed by tuning the polarization of the excitation light. First, we demonstrated theoretically that the plasmonic near-field near a single AuNP is variable under different illumination polarizations in an FDTD simulation. TIR-FCS was then used to characterize the behavior of molecule fluorescence within the plasmonic near-field volume to reveal the plasmonic near-field. The experimental results show that variation in the plasmonic near-field affects ACF curves, which agrees quantitatively with the theoretical analysis. These results are highly relevant to important efforts to clarify the plasmonic near-field of a metallic nanostructure and the interaction between emitters and a plasmonic antenna. Additionally, they can be used to improve TIR-based biological imaging techniques, such as by designing a TIR fluorescence microscopy configuration combined with a thin metallic film or a nanoparticle array.

This work was supported by the National Natural Science Foundation of China (Grant no. 61008026, 11121091 and 90921008) and the National Basic Research Program of China (Grant no. 2007CB307001 and 2009CB930504).

Notes and references

1 J. A. Schuller, E. S. Barnard, W. Cai, Y. C. Jun, J. S. White and M. L. Brongersma, *Nat. Mater.*, 2011, **9**, 193–204.
2 J. N. Anker, W. P. Hall, O. Lyandres, N. C. Shah, J. Zhao and R. P. Van Duyne, *Nat. Mater.*, 2008, **7**, 442–453.
3 H. A. Atwater and A. Polman, *Nat. Mater.*, 2010, **9**, 205–213.
4 X. Zhang and Z. Liu, *Nat. Mater.*, 2008, **7**, 435–441.
5 T. Hartling, P. Reichenbach and L. M. Eng, *Opt. Express*, 2007, **15**, 12806–12817.
6 S. Kuhn, U. Hakanson, L. Rogobete and V. Sandoghdar, *Phys. Rev. Lett.*, 2006, **97**, 017402.
7 P. Anger, P. Bharadwaj and L. Novotny, *Phys. Rev. Lett.*, 2006, **96**, 113002.
8 M. Achermann, K. L. Shuford, G. C. Schatz, D. H. Dahanayaka, L. A. Bumm and V. I. Klimov, *Opt. Express*, 2007, **32**, 2254–2256.
9 R. Vogelgesang, J. Dorfmüller, R. Esteban, R. T. Weitz, A. Dmitriev and K. Kern, *Phys. Status Solidi B*, 2008, **245**, 2255–2260.
10 F. J. Garcia de Abajo, *Rev. Mod. Phys.*, 2010, **82**, 209–275.
11 S. M. Novikov, J. Beermann, T. Sondergaard, A. E. Boltasseva and S. I. Bozhevolnyi, *J. Opt. Soc. Am. B*, 2009, **26**, 2199–2203.
12 M. V. Bashevoy, F. Jonsson, A. V. Krasavin, N. I. Zheludev, Y. Chen and M. I. Stockman, *Nano Lett.*, 2006, **6**, 1113–1115.
13 E. J. R. Vesseur, R. de Waele, M. Kuttge and A. Polman, *Nano Lett.*, 2007, **7**, 2843–2846.
14 A. Taflove and S. C. Hagness, *Computational Electrodynamics: the Finite-Difference Time-Domain Method*, Artech House, Norwood, MA, 3rd edn, 2005.
15 D. Magde, E. Elson and W. W. Webb, *Phys. Rev. Lett.*, 1972, **29**, 705–708.
16 L. Kastrup, H. Blom, C. Eggeling and S. W. Hell, *Phys. Rev. Lett.*, 2005, **94**, 178104.
17 H. Rigneault, J. Capoulade, J. Dintinger, J. Wenger, N. Bonod, E. Popov, T. W. Ebbesen and P.-F. Lenne, *Phys. Rev. Lett.*, 2005, **95**, 117401–117404.
18 M. J. Levene, J. Korlach, S. W. Turner, M. Foquet, H. G. Craighead and W. W. Webb, *Science*, 2003, **299**, 682–686.
19 T. Sande, R. Wyss, C. Santschi, G. Hassaie, C. Deluz, O. Martin, S. Wennmalm and H. Vogel, *Nano Lett.*, 2012, **12**, 370–375.
20 L. C. Estrada, P. F. Aramendía and O. E. Martínez, *Opt. Express*, 2008, **16**, 20597–20602.
21 P. Winckler, R. Jaffiol, J. Plain and P. Royer, *J. Phys. Chem. Lett.*, 2010, **1**, 2451–2454.
22 Q. Wang, G. Lu, L. Hou, T. Zhang, C. Luo, H. Yang, G. Barbillon, F. H. Lei, C. A. Marquette, P. Perriat, O. Tillement, S. Roux, Q. Ouyang and Q. Gong, *Chem. Phys. Lett.*, 2011, **503**, 256–261.
23 G. Frens, *Nat. Phys. Sci.*, 1973, **241**, 20.
24 K. C. Grabar, P. C. Smith, M. D. Musick, J. A. Davis, D. G. Walter, M. A. Jackson, A. P. Guthrie and M. J. Natan, *J. Am. Chem. Soc.*, 1996, **118**, 1148–1153.
25 K. Hassler, T. ANhut, R. Rigler, M. Gösch and T. Lasser, *Biophys. J.*, 2005, **88**, L01–L03.
26 N. L. Thompson and B. L. Steele, *Nat. Protoc.*, 2007, **2**, 878–890.
27 G. Lu, T. Zhang, W. Li, L. Hou, J. Liu and Q. Gong, *J. Phys. Chem. C*, 2011, **115**, 15822–15828.
28 D. Axelrod, *Traffic*, 2001, **2**, 764–774.
29 Y. Sako and T. Uyemura, *Cell Struct. Funct.*, 2002, **27**, 357.
30 T. P. Burghardt, J. E. Charlesworth, M. F. Halstead, J. E. Tarara and K. Ajtai, *Biophys. J.*, 2006, **90**, 4662–4671.

